Theoretical strength and charge redistribution of fcc Ni in tension and shear

2008 J. Phys.: Condens. Matter 20 335216

(http://iopscience.iop.org/0953-8984/20/33/335216)

J. Phys.: Condens. Matter **20** (2008) 335216 (8pp) doi:10.1088/0953-8984/20/33/335216

Theoretical strength and charge redistribution of fcc Ni in tension and shear

Yue-Lin Liu[1], Ying Zhang[1], Hong-Bo Zhou[1], Guang-Hong Lu[1,3] and Masanori Kohyama[2]

[1] School of Science, Beijing University of Aeronautics and Astronautics, Beijing 100083, People's Republic of China
[2] Research Institute of Ubiquitous Energy Devices, National Institute of Advanced Industrial Science and Technology, Osaka 563-8577, Japan

E-mail: LGH@buaa.edu.cn

Received 25 April 2008, in final form 10 July 2008
Published 28 July 2008
Online at stacks.iop.org/JPhysCM/20/335216

Abstract

We employ a first-principles total-energy method to investigate the theoretical tensile and shear strengths of fcc Ni systematically. The theoretical tensile strengths are shown to be 36.1, 10.5 and 34.1 GPa in the [001], [110] and [111] directions, respectively. We indicate that [110] is the weakest direction due to the formation of an instable bct 'phase' in the tensile process. The theoretical shear strengths are, respectively, 5.1 and 15.8 GPa in the 'easy' and 'hard' directions in the $\{111\}\langle 112\rangle$ slip system, and 6.4 GPa in the $\{111\}\langle 110\rangle$ slip system. Both the tensile and the shear strengths are consistent with either experimental or theoretical values. The different shear strengths in the 'easy' and 'hard' directions originate from the different charge redistribution under the shear strain. The shear strain along the 'easy' direction of [112] results in a charge distributed in the $\langle 001\rangle$ which forms a directional bond, while the strain along the 'hard' direction of [112] makes the charge extend to the whole {111} interlayers.

(Some figures in this article are in colour only in the electronic version)

1. Introduction

The theoretical (ideal) strength of materials is the stress that is required to force deformation or fracture at the elastic instability [1]. The theoretical strength sets an upper bound on the attainable stress. The strength of a real crystal can be changed by the existing cracks, dislocations, grain boundaries and other microstructural features, but its theoretical value can never be increased [1, 2]. The theoretical tensile strength is when a material becomes unstable with respect to fracture by the spontaneous separation of atomic planes. On the other hand, the theoretical shear strength is when a material becomes unstable with respect to spontaneous shear deformation. The upper limit of the tensile or shear strength is of obvious interest for strong solids in atomic models [1, 3–5]. These models were originally developed by Frenkel [6] and Orowon [7], since the theoretical strength is an intrinsic material property that is determined by the behavior of valence electrons and ions.

By virtue of the development of the density-functional theory (DFT) [8, 9] combined with the band-theoretical schemes and the rapid progress of modern computers, it became possible to do a first-principles computational tensile or shear test (FPCTT/FPCST) to investigate the stress as a function of strain and obtain the theoretical tensile or shear strengths by deforming crystals to failure [10]. In FPCTT/FPCST, symmetry is generally an important factor in determining the stress–strain relation and the calculated theoretical strength. For single crystals, earlier studies on the theoretical tensile strength of W, Cu, Ir and NiAl have been made by Sob *et al* [11–13]. So far, the theoretical tensile and shear strengths of fcc (Cu, Al) and bcc (Mo, W, Nb, Fe) metals have been published [2, 5, 14, 15]. On the other hand, the theoretical strength can also be extended to defective systems containing only one defect such as a point defect [16], an interface or a grain boundary [17–23]. The theoretical tensile strengths of a clean Al grain boundary (GB) and an Al GB containing Na, Ca, S and Ga have

[3] Author to whom any correspondence should be addressed.

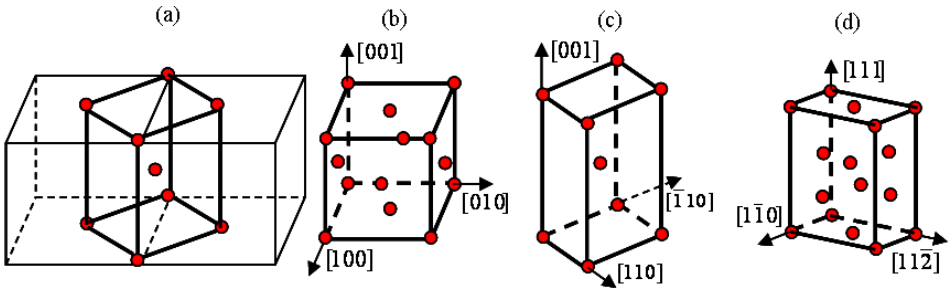

Figure 1. The geometric structure of tensile unit cells of the fcc Ni in the directions [001] and [110]. (a) shows the body-centered tetragonal (bct) unit cell inside the fcc Ni. (b) is a general fcc unit cell of Ni with 4 atoms inside, while (c) is a bct unit cell with 2 atoms inside drawn from (a). The unit cell of (c) is used for the FPCTT in the [110] direction, and both (b) and (c) can be used for the FPCTT in the [001] direction. (d) is the unit cell containing 6 atoms employed for the FPCTT in the [111] direction.

been calculated in order to explore the impurity-induced intergranular embitterment [19–23].

Ni is one of the important magnetic transition metals which have many applications. So far, the FPCST has been done by Ogata *et al* to calculate the theoretical shear strength in the 'easy' shear direction in the $\{111\}\langle 112\rangle$ slip system [24]. However, the stress as a function of strain and the theoretical strength (both tensile and shear) for Ni have not been systematically explored. In particular, little has been done on the charge distribution in the shear process in both 'easy' and 'hard' directions in the $\{111\}\langle 112\rangle$ slip systems, which can reflect the intrinsic nature of the atomic bonding of Ni. Further, the theoretical (ideal) tensile and shear strengths of fcc Ni have been provided either experimentally (i.e. estimated from the experimentally determined elastic constants) or theoretically (e.g. estimated from the potential energy) [1], making us able to make a full comparison. In this paper, we thus have performed both the FPCTT and the FPCST on fcc Ni to explore its theoretical mechanical properties systematically.

2. Computational method

We employ a total-energy method based on the density-functional theory (DFT) [25, 26] with the generalized gradient approximation (GGA) [27]. The wavefunctions are obtained by solving the Kohn–Sham equation using a plane-wave basis. The plane-wave kinetic energy cutoff is 340 eV. For summation over the Brillouin zone, a uniform grid of k points is chosen according to the Monkhorst–Pack scheme [28]. All calculations have been performed using the VASP code [29, 30]. The spin polarization has been taken into account because Ni is a typical magnetic transition metal. The theoretical shear strength can be lowered without spin polarization [24]. The interaction between ions and electrons is described by the projector augmented wave (PAW) potential based on GGA. The energy relaxation iterates until the forces on all the atoms are less than 10^{-3} eV Å^{-1}.

The calculated equilibrium lattice parameter is 3.519 Å for fcc Ni, in good agreement with the corresponding experimental value of 3.52 Å. The fcc Ni has three independent components for the elastic constant, i.e. C_{11}, C_{12} and C_{44}. All these three components have been calculated. As shown in table 1, the calculated elastic constants are consistent with those from experiment [31]. For instance, C_{11} was calculated to be 283.6 GPa, ∼8% larger than the 261.2 GPa from experiment.

Table 1. Calculated and experimental elastic constants of fcc Ni.

Elastic constant (GPa)	Calculation	Experimental [31]
C_{11}	283.6	261.2
C_{12}	157.7	150.8
C_{44}	126.8	131.7

In the FPCTT/FPCST, a tensile (uniaxial) or shear strain has been applied to the chosen crystalline directions of fcc Ni, and the corresponding stress is calculated according to the Nielsen–Martin scheme [32]. For the uniaxial tensile strain, the tensile stress σ is calculated from

$$\sigma = \frac{1}{\Omega(\varepsilon)}\frac{\partial E}{\partial \varepsilon}, \tag{1}$$

where E is the total energy and $\Omega(\varepsilon)$ is the volume at a given tensile strain of ε. Similar to the previous study on Mo [5], the shear stress τ corresponding to the shear strain is

$$\tau = \frac{1}{\Omega(\gamma)}\frac{\partial E}{\partial \gamma}, \tag{2}$$

where $\Omega(\gamma)$ is the volume at a given shear strain of γ.

The lattice vectors were incrementally added in the direction of the imposed strain. At each strain step, the structure was fully relaxed until all the other five stress components vanished except those in the tensile or shear direction. The tensile or shear stress for each strain step can be calculated, and thus the stress–strain relation and the theoretical tensile or shear strength can be obtained.

3. Results and discussion

3.1. FPCTT of fcc Ni and the theoretical tensile strength

In the FPCTT of fcc Ni, we choose three representative directions including [001], [110] and [111]. Two unit cells with different symmetry are employed for the FPCTT in different directions, as shown in figure 1.

For the FPCTT in the [001] direction, both unit cells of (b) and (c) in figure 1 can be used. Here we used the body-centered tetragonal (bct) unit cell that is drawn from the fcc crystal. The original unit cell exhibits tetragonal symmetry. Such symmetry

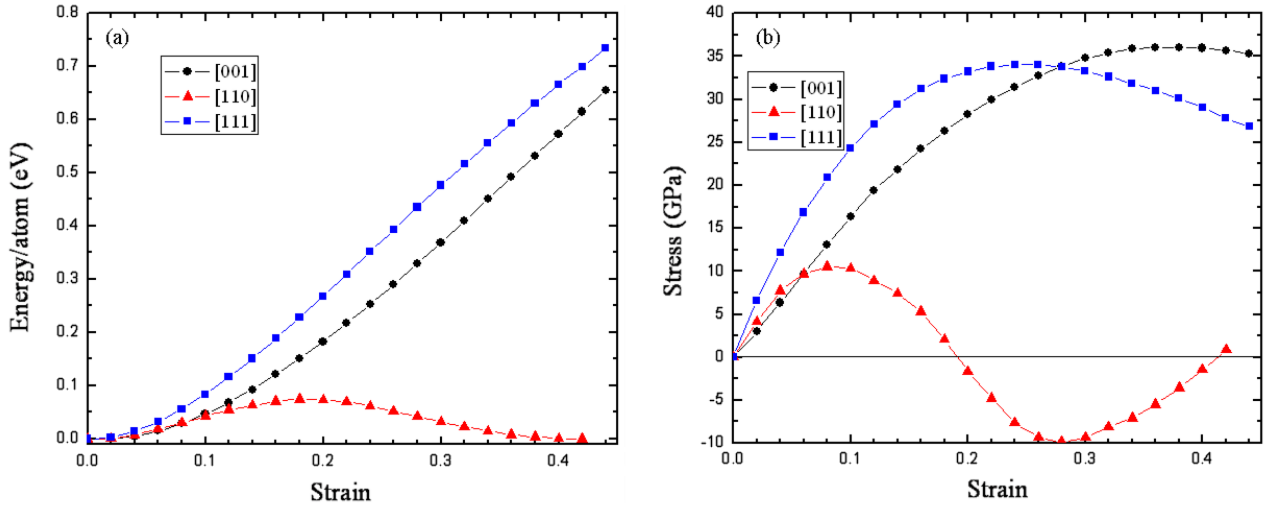

Figure 2. Energy (a) and stress (b) as a function of tensile strain in the [001], [110] and [111] directions, respectively.

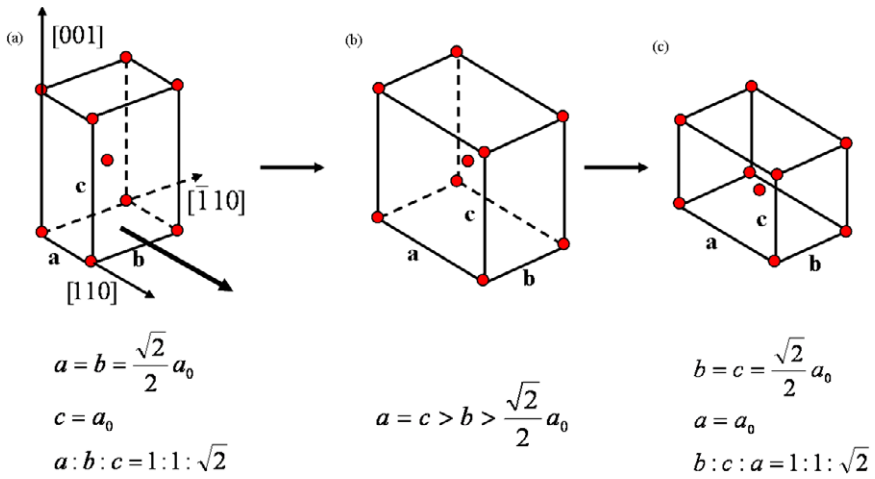

Figure 3. The evolution of geometric structures of the unit cell of fcc Ni under tension in the [110] direction.

will not change in the tensile process in the [001] direction. Figure 2(a) shows the strain energy as a function of tensile strain. The strain energy increases with the increasing strain, exhibiting an inflection at the strain of 38%. Correspondingly, as shown in figure 2(b), the stress increases with increasing strain until it reaches a maximum of 36.1 GPa at a strain of 38%, after which the stress decreases. Thus, the theoretical tensile strength is 36.1 GPa in the ⟨001⟩ direction.

Next, we performed the FPCTT in the [111] direction, the unit cell of which is shown in figure 1(d). Similar to the [001] direction, figure 2(b) shows the stress reaches the maximum of 34.1 GPa at a strain of 24%, corresponding to the inflection in the energy–strain curve (figure 2(a)). The theoretical tensile strength is thus 34.1 GPa in the [111] direction.

As compared with the [001] and [111] directions, the stress–strain relation in the [110] direction differs noticeably. The unit cell we used for this direction is the bct shown in figure 1(c). The strain energy as a function of strain is shown in figure 2(a). The energy increases first with increasing strain, then reaches a maximum at a strain of 18%, after which the energy decreases to zero again at a strain of 42%. The maximum or minimum of the strain energy corresponds to zero-stress points in the stress–strain curve in the [110] direction. As shown in figure 2(b), the stress exhibits one maximum of 10.5 GPa at a strain of 8%, and then reaches zero at the strain of 18%. Further strain increase leads to a negative stress, and the stress reaches a minimum of 9.9 GPa at a strain of 28%. It reaches zero again at a strain of 42%. Therefore, the stress exhibits two saddle points (one maximum and one minimum) and three zero points in the tensile process so far.

The zero-stress point in the stress–strain curve corresponds to a stress-free phase generated in the tensile process. The initial zero-stress point corresponds to the initial bct phase (fcc structure), as shown in figure 3(a). The ratio of a:b:c for such a phase is $1{:}1{:}\sqrt{2}$. With strain increasing, the lattice parameter of a increases, while c decreases and b remains almost unchanged, as shown in figure 4. The lattice parameter of c is equivalent with a at the strain of 18%, where the stress reaches the second zero-stress point. At this point, there forms a new bct structure with $a = c > b$ (figure 3(b)), different

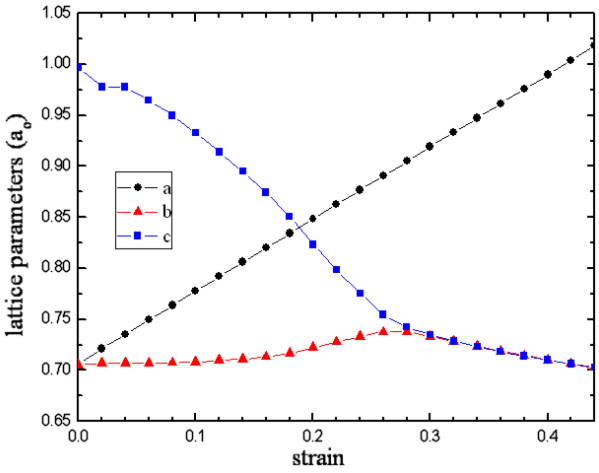

Figure 4. The lattice parameter in units of a_0 as a function of tensile strain in the [110] direction.

from the original one. This point corresponds to the saddle point of the energy maximum (figure 2(a)), which indicates the new bct structure is an instable 'phase' despite its stress-free characteristic. Such a structure will evolve to other stable phases, even with a small perturbation. With further increase of strain, the lattice parameter of c decreases continuously and becomes equal to b at a strain of ∼32%. The ratio of b:c:a becomes 1:1:$\sqrt{2}$ at the strain of 42% (figure 3(c)), corresponding to the third zero-stress point in the stress–strain curve. The present stress-free bct structure (i.e. fcc structure) is actually the same as the initial one (figure 3(a)), but with a rotation of 90°. Consequently, the stress–strain relation after the strain of 42% should be exactly the same as that in the [001] direction shown in figure 2.

The evolution of the cell geometry shown in figure 3 is similar to the 'orthorhombic path', as investigated in several previous studies [2, 15]. It should be noted that the tensile process between the strains of 18% and 42% with negative stress for the [110] direction is a *virtual* process and cannot actually occur. In the real process, the bct structure in the strain of 18% (figure 3(b)) will evolve automatically to the final bct structure at the strain of 42% (figure 3(c)).

According to the above results, both [001] and [111] can be considered as stronger directions with the theoretical tensile strength as large as above (30 GPa). However, [110] is obviously a weak direction with tensile strength only ∼10 GPa, despite it being a most-closely-packed crystalline direction in the fcc Ni. The reason lies in that there forms an instable bct 'phase' (saddle-point structure) in the tensile process in the [110] direction, as depicted above.

3.2. FPCST of fcc Ni and the theoretical shear strength

In addition to the tensile process and the theoretical tensile strength, the shear process and the theoretical shear strength are also quite particular for the metals. We have thus performed the FPCST for the fcc Ni, choosing the slip systems including {111}⟨112⟩ and {111}⟨110⟩, which are two representative slip systems for fcc metals such as Ni. Although the shear process in the ⟨112⟩ direction is preferred to occur in the actual shear process [33] due to the lower generalized stacking fault (GSF) energy, we still perform the FPCST in the {111}⟨110⟩ slip system for reference.

For fcc metals, shear deformation in the {111}⟨112⟩ slip system can produce two different kinds of saddle-point structures, i.e. the stress–strain relation of $\{111\}[11\bar{2}]$ differs from that in the opposite direction of $\{111\}[\bar{1}\bar{1}2]$. The two shear deformations are called the 'easy' and 'hard' shear directions, respectively. But, for the {111}⟨110⟩ slip system, the stress–strain relation in all shear directions is symmetric.

The energy–strain and stress–strain curves for the {111}⟨112⟩ slip system are shown in figure 5. For the $\{111\}[11\bar{2}]$ shear direction, the strain energy increases first as the strain increases, then exhibits an inflection at a strain of 12%, and reaches the energy maximum at a strain of 32%. Correspondingly, the stress reaches its maximum of 5.1 GPa

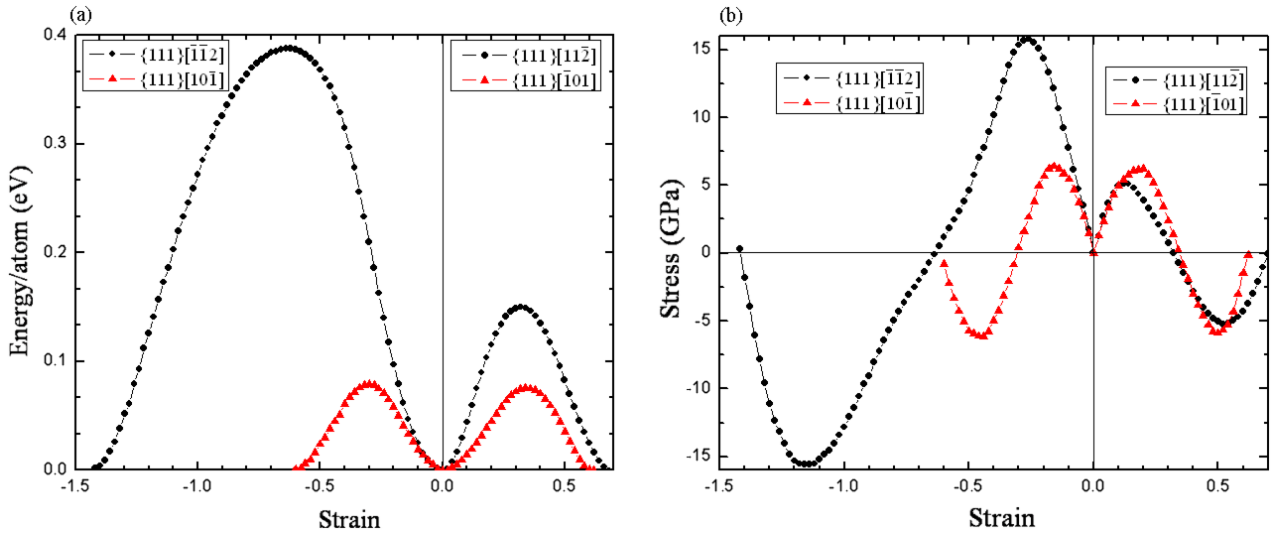

Figure 5. Energy (a) and stress (b) as a function of shear strain in the {111}⟨112⟩ and {111}⟨110⟩ slip systems, respectively.

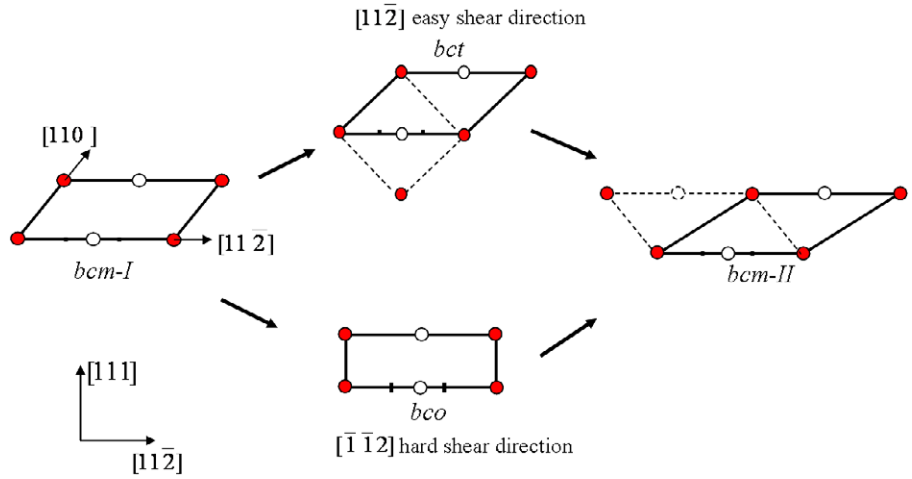

Figure 6. The evolution of geometric structure (top view from the [1$\bar{1}$0] direction) starting from the bcm-I structure in the shear process in the {111}[11$\bar{2}$] easy and {111}[$\bar{1}\bar{1}$2] hard slip directions. The bct (one saddle-point structure) appears in the easy direction, while the bco (another saddle-point structure) appears in the hard direction. The bcm-II (base-centered monoclinic) exhibits the same structure and symmetry as the original bcm-I structure with the same lengths of the two sides, but it should be viewed from the opposite direction, i.e. [$\bar{1}$10] (the dashed line of bcm-II). The red filled and white open circles represent the atoms in the different [1$\bar{1}$0] planes.

at the strain of 12% and becomes zero at a strain of 32%, after which the stress becomes negative. Thus, the theoretical shear stress is 5.1 GPa for the {111}[11$\bar{2}$] direction. For the {111}[$\bar{1}\bar{1}$2] shear direction, the energy–strain and stress–strain curves are similar to those of the {111}[11$\bar{2}$] direction, but the theoretical shear strength is 15.8 GPa at a strain of 26%. The shear strength of 15.8 GPa in the {111}[11$\bar{2}$] direction is roughly three times larger than that of 5.1 GPa in the {111}[11$\bar{2}$] direction. Thus, we call {111}[11$\bar{2}$] as the 'easy' direction and {111}[$\bar{1}\bar{1}$2] as the 'hard' direction. Hence, the theoretical shear strength for the {111}⟨112⟩ slip system is 5.1 GPa, corresponding to the easy direction, which agrees well with 5.05 GPa calculated by Ogata *et al* [24].

The geometric structure evolves quite differently between the 'easy' and 'hard' directions in the {111}⟨112⟩ slip system. Initially the fcc unit cell can be treated as a base-centered monoclinic (bcm) structure with the lengths of the two sides as $0.71a_0$ (a_0 is the lattice parameter of fcc Ni) and $1.22a_0$, respectively (bcm-I in figure 6). Under the shear in the 'easy' {111}[11$\bar{2}$] direction, a stress-free bct structure (saddle-point structure) appears at the strain of 32% (bct in figure 6, depicted as the dashed line), while another stress-free bcm structure appears at the strain of 68% (bcm-II in figure 6). The bcm-II structure exhibits the same structure and symmetry as the original bcm-I structure with the same lengths of the two sides ($0.71a_0$ and $1.22a_0$), but it should be viewed from the opposite direction, i.e. [$\bar{1}$10] (the dashed line of bcm-II). Under the shear in the 'hard' {111}[$\bar{1}\bar{1}$2] direction, a stress-free base-centered orthorhombic (bco) structure (saddle-point structure) appears at the strain of 64% (bco in figure 6); while the structure evolves to the bcm-II structure at the strain of 142%.

As illustrated in figure 6, successive shear in the easy direction results in the same stress–strain relation as in the hard direction, and vice versa. Consequently, there forms a cycle of bcm-I ↔ bct ↔ bcm-II ↔ bco ↔ bcm-I characterized by the appearance of the 'easy' and 'hard' stress–strain relations alternately under the shear in either {111}[11$\bar{2}$] or {111}[$\bar{1}\bar{1}$2]. This demonstrates again that the 'easy' direction for the fcc Ni is {111}[11$\bar{2}$] and the 'hard' direction is {111}[$\bar{1}\bar{1}$2].

The energy and stress as a function of the shear strain in the {111}⟨110⟩ slip system are shown in figure 5. Different from the {111}⟨112⟩ slip system, the two {111}[$\bar{1}\bar{1}$0] and {111}[110] shear directions are symmetric, and thus exhibit no 'hard' and 'easy' directions. The theoretical shear strength of the {111}⟨110⟩ slip system is 6.2 GPa at a strain of 20%, which is a little larger than the 5.1 GPa of the {111}⟨112⟩ system. This is because the GSF energy in the ⟨110⟩ direction is larger than in the ⟨112⟩ direction for fcc metals [14, 33] and thus easier to slip under the shear deformation.

In addition, the theoretical shear strength in the {111}⟨112⟩ slip system (5.1 GPa) is lower than the theoretical tensile strength of 10.5 GPa in the [110] direction, which indicates that the slide is easier to occur. This suggests Ni is a metal with good plasticity.

3.3. Charge redistribution in the FPCST and its relation with the shear strength

We next investigate the charge density distribution in Ni in the process of FPCST. The charge density iso-surface maps for the 'easy' and 'hard' shear directions, i.e. {111}[11$\bar{2}$] and{111}[$\bar{1}\bar{1}$2], are shown in figure 7. It is clear to see that the charge density distributions are quite different for the two slip directions. For the easy direction, the charge density will distribute along the ⟨001⟩ direction with the strain increasing, which can lead to directional bonding in the ⟨001⟩ direction (figures 7(a)–(c)). This bonding characteristic is similar to another typical fcc metal, Al [14]. In contrast, the charge goes to distribute between the {111} crystalline planes with strain increasing (figures 7(a) → (b′) → (c′)) and extends to the full {111} interlayer at the strain of 26% (figure 7(c′)). This will make the interaction between the {111} crystalline planes

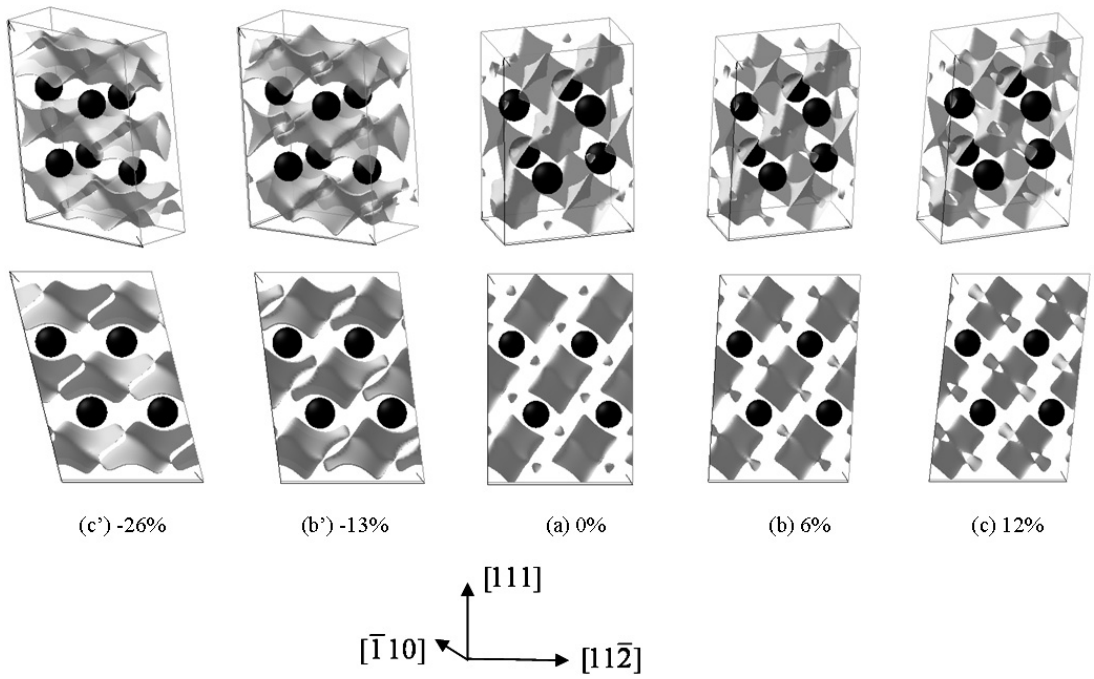

Figure 7. Charge density iso-surface distribution at the different shear strains for the {111}[11$\bar{2}$] easy and {111}[$\bar{1}\bar{1}$2] hard shear directions, respectively. Negative strain represents the hard shear direction. The lower panel is a side view of the upper panel from the [1$\bar{1}$0] direction.

much stronger as compared with the easy direction. Such a characteristic of the charge redistribution under the shear strain results in the much higher shear strength in the hard shear direction in comparison with the easy direction.

The different charge redistribution in the shear process between the easy and hard directions is due to the shear anisotropy in these two directions. Namely, the bcm-I structure evolves to a bct structure in the easy direction, while it evolves to a bco structure in the hard direction.

The theoretical shear strength of Ni in the easy direction is 5.1 GPa. As compared with those of Al and Cu in the same slip system, which are 2.84 and 2.15 GPa, respectively [14], the strength of Ni is higher. This should originate from the electronic structure difference between them. The valence electrons of Ni are described as $3d^8 4s^2$, with eight electrons in the d orbital that is not fully occupied, which contribute largely to its much higher shear strength under the shear strain. Cu is characterized by one fully occupied 3d orbital with ten electrons and one 4s orbital with only one electron, making the electrons localize around the atoms even under the shear strain [14]. Al is an element that is between the metals and nonmetals, and has an electronic structure of $3s^2 3p^1$. Al can form strong directional bonds containing covalent components with less-coordinated atoms such as under the tensile or shear strain [14], or for defects including vacancy [33, 34], surface [35] or grain boundary [18]. Hence, the shear strength of Al is higher than that of Cu, but both are lower than that of Ni.

3.4. Comparison with the experiments

Theoretically, both the theoretical tensile and shear strengths can be determined from the Young's modulus and shear modulus. These moduli can be calculated from the elastic constants [1]. Here we first calculate the Young's modulus and shear modulus from the elastic constants determined from the present calculations (table 1) and compare them with those from experiment.

Table 2. The theoretical tensile strengths from our calculation and other methods, Young's modulus from our calculation and experiments in the [001], [110] and [111] directions, respectively.

Direction	Calc. σ_m (GPa)	σ_m [a]	Calc. E (GPa)	Expt[b] E (GPa)
[001]	36.1	37	170.9	150.8
[110]	10.5		259.6	237.8
[111]	34.1		313.9	320.2

[a] Polanyi and Orowan [1].
[b] Calculated analytically from experimental elastic constants in table 1.

The Young's moduli in the [001], [110] and [111] directions are calculated to be 170.9, 259.6, and 313.9 GPa, respectively. These moduli are consistent with the experimental value, as shown in table 2. The theoretical tensile strength in the [001] direction of fcc Ni is 36.1 GPa according to the present calculation. This agrees well with 37 GPa estimated from the method by Polanyi and Orowan [1], i.e. $\sigma = \sqrt{E\gamma/a_0}$, which depends on the experimental values of surface energy γ and Young's modulus E.

In spite of the different shear paths, the stress–strain curves coincide in the original shear stage for the two slip systems according to the present calculation (figure 5(b)). We can thus estimate the shear modulus from the slope at the start of the stress–strain curves for both the ⟨112⟩ and ⟨110⟩ directions. The shear modulus is calculated

Table 3. Shear modulus G, theoretical shear stress τ_m and failure strain τ_m/G in different slip systems.

	G (GPa)			τ_m (GPa)		τ_m/G	
Slip system	Calc.	Theory[d]	Expt[e]	Calc.	Theory[d]	Calc.	Theory[d]
{111}⟨112⟩	84.1[a]	62	77.8	5.1[a]	7.1	0.061[a]	0.114
	63.9[b]					0.080[b]	
	60.1[c]			5.05[c]		0.084[c]	
{111}⟨110⟩	84.1[a]		77.8	6.2[a]		0.074[a]	
	63.9[b]						

[a] The present calculation.
[b] The present calculation from the slope of the stress–strain curve.
[c] Calculation value from [31].
[d] Calculation from Mackenzie's method [1].
[e] The experimental value (calculation from the experimental elastic constants).

to be 63.9 GPa. For the ⟨112⟩ direction, this is consistent with the experimental value of 68.5 GPa determined from experimental elastic constants [26] and the theoretical value of 62 GPa based on Mackenzie's scheme [1] (table 3). This also agrees with 60.1 GPa calculated by Ogata *et al* [24].

On the other hand, the shear modulus can also be determined from the calculated elastic constants in the present calculation in table 1. We derive the formulation of G as

$$G_{\langle 112\rangle} = G_{\langle 110\rangle} = \frac{2C_{44}(C_{11} - C_{12})}{2C_{44} + C_{11} - C_{12}}. \quad (3)$$

The results are 84.1 GPa for both ⟨112⟩ and ⟨110⟩, which are consistent with the experimental values of 77.8 GPa for both directions calculated from the experimentally determined elastic constants [31].

The simplest calculation of theoretical shear strength originates from Frenkel [6], who presumes two neighboring planes with a repeat distance in the shear direction in a crystal. However, this is a very rough estimation. A more accurate description of the theoretical shear strength has been proposed by Mackenzie [1], who has chosen a convenient potential energy function and matches the suitable coefficients according to different metals, and then deduced the shear stress, i.e. derivation of potential energy. This method is shown to be able to give reasonable values of the theoretical shear strengths for fcc metals. The theoretical shear strength for {111}⟨112⟩ is shown to be 5.1 GPa, corresponding to the easy direction of fcc Ni in the present work. This is in good agreement with the result by Ogata *et al* [24], but lower than 7.1 GPa determined from Mackenzie's scheme [1]. This may be due to the full geometry relaxation in the present FPCST in the shear process in comparison with Mackenzie's scheme. Such a geometry relaxation effect has also been observed in both simulation and experimental studies [36–40]. Furthermore, the calculated failure strains (τ_m/G) are also shown in table 3.

4. Conclusions

We employ the first-principles total-energy method based on the density-functional theory with the Generalized Gradient Approximation to investigate the theoretical tensile and shear strengths of fcc Ni systemically. The theoretical tensile strengths are shown to be 36.1, 10.5 and 34.1 GPa in the [001], [110] and [111] directions, respectively. We indicate that [110] is a weakest direction due to the formation of an unstable bct 'phase' in the tensile process. The theoretical shear strengths are, respectively, 5.1 and 15.8 GPa in the 'easy' and 'hard' directions in the {111}⟨112⟩ slip system, and 6.4 GPa in the {111}⟨110⟩ slip system. Both the tensile and the shear strengths are consistent with either experimental or theoretical values. The different shear strengths in the 'easy' and 'hard' directions originate from the different charge redistribution under the shear strain. Namely, the shear strain makes the charge distributed in the ⟨001⟩ direction to form a directional bond for the {111}[11$\bar{2}$] direction, which makes it extend to the whole {111} interlayers along the shear direction due to its electronic structure characterized by the 3d orbital that is not fully occupied. The results provide a good reference for understanding the intrinsic mechanical properties of Ni as well as other fcc metals.

Acknowledgments

The research is supported by the National Natural Science Foundation of China (NSFC) with grant no. 50771008 and the New Century Excellent Talents in University.

References

[1] Kelly A and Macmillan N H 1986 *Strong Solids* 3rd edn (Oxford: Clarendon)
[2] Luo W, Roundy D, Cohen M L and Morris J W Jr 2002 *Phys. Rev.* B **66** 094110
[3] Polanyi M 1921 *Z. Phys.* **7** 323
[4] Frenkel J 1926 *Z. Phys.* **37** 572
[5] Roundy D, Krenn C R, Cohen M L and Morris J W Jr 1999 *Phys. Rev. Lett.* **82** 2713
[6] Frenkel J 1926 *Z. Phys.* **7** 323
[7] Orowon E 1949 *Rep. Prog. Phys.* **12** 185
[8] Hohenberg G P and Kohn W 1964 *Phys. Rev.* **136** B864
[9] Kohn W and Sham L J 1965 *Phys. Rev.* **140** A1133
[10] Morris J W Jr and Krenn C R 2000 *Phil. Mag.* A **80** 2827
[11] Sandera P, Pokluda J, Wang L G and Sob M 1997 *Mater. Sci. Eng.* A **234–236** 370
[12] Sob M, Wang L G and Vitek V 1997 *Mater. Sci. Comput.* A **234–236** 1075
[13] Sob M, Wang L G and Vitek V 1998 *Phil. Mag.* B **78** 653

[14] Ogata S, Li J and Yip S 2002 *Science* **298** 807
[15] Clatterbuck D M, Chrzan D C and Morris J W Jr 2003 *Acta Metall.* **51** 2271
[16] Deyirmenjian V B, Heine V, Payne M C, Milman V, Lynden-Bell R M and Finnis M W 1995 *Phys. Rev.* B **52** 15191
[17] Kohyama M 1999 *Phil. Mag. Lett.* **79** 659
[18] Kohyama M 2002 *Phys. Rev.* B **65** 184107
[19] Lu G-H, Deng S H, Wang T M, Kohyama M and Yamamoto R 2004 *Phys. Rev.* B **69** 134106
[20] Lu G-H, Zhang Y, Deng S, Wang T, Kohyama M, Yamamoto R, Liu F, Horikawa K and Kanno M 2006 *Phys. Rev.* B **73** 224115
[21] Zhang Y, Lu G-H, Wang T, Deng S, Kohyama M and Yamamoto R 2006 *Mater. Trans.* **47** 2678
[22] Zhang Y, Lu G-H, Hui X L, Wang T, Kohyama M and Yamamoto R 2007 *J. Phys.: Condens. Matter* **19** 456225
[23] Zhang Y, Lu G-H, Deng S, Wang T, Xu H, Kohyama M and Yamamoto R 2007 *Phys. Rev.* B **75** 174101
[24] Ogata S, Li J, Hirosaki N, Shibutani Y and Yip S 2003 *Phys. Rev.* B **68** 184103
[25] Hohenberg G P and Kohn W 1964 *Phys. Rev.* **136** B864
[26] Kohn W and Sham L J 1965 *Phys. Rev.* **140** A1133
[27] Perdew J P and Wang Y 1992 *Phys. Rev.* B **45** 13244
[28] Monkhorst H J and Pack J D 1976 *Phys. Rev.* B **13** 5188
[29] Kresse G and Hafner J 1993 *Phys. Rev.* B **47** 558
[30] Kresse G and Furthmüller J 1996 *Phys. Rev.* B **54** 11169
[31] Kittel C 1996 *Introduction to Solid State Physics* (New York: Wiley)
[32] Nielsen O H and Martin R M 1985 *Phys. Rev.* B **32** 3780
Nielsen O H and Martin R M 1987 *Phys. Rev.* B **35** 9308
[33] Lu G, Kioussis N, Bulatov V V and Kaxiras E 2000 *Phys. Rev.* B **62** 3099
[34] Carling K, Wahnstrum G, Mattsson T R, Mattsson A E, Sandberg N and Grimvall G 2000 *Phys. Rev. Lett.* **85** 3862
[35] Uesugi T, Kohyama M and Higashi K 2003 *Phys. Rev.* B **68** 184103
[36] Loffler J and Weissmuller J 1995 *Phys. Rev.* B **52** 076
[37] Qin X Y, Zhang X R, Cheng G S and Zhang L D 1998 *Nanostruct. Mater.* **4** 661
[38] Hasnaoui A, Van Swygenhoven H and Derlet P M 2002 *Acta Mater.* **50** 3927
[39] Kumar K S, Van Swygenhoven H and Suresh S 2003 *Acta Mater.* **51** 5743
[40] Karakasidis T E, Charitidis C A, Skarakis D and Chouliaras F 2007 *Surf. Sci.* **601** 3521